

# Dislocation Dynamics in Rayleigh-Bénard Convection

Th. Walter<sup>1</sup>, W. Pesch<sup>1</sup>, and E. Bodenschatz<sup>2</sup>

<sup>1</sup> *Physikalisches Institut der Universität Bayreuth, D-95440 Bayreuth*

<sup>2</sup> *Laboratory of Atomic and Solid State Physics, Cornell University, Ithaca, NY 14853*

(Dated: November 13, 2018)

Theoretical results on the dynamics of dislocations in Rayleigh-Bénard convection are reported both for Swift-Hohenberg models and the Boussinesq equations. For intermediate Prandtl numbers the motion of dislocations is found to be driven by the superposition of two independent contributions: (i) the Peach-Koehler force derived from the change of a Lyapunov potential with pattern wave number; (ii) a non-potential advection force on the dislocation core by its self-generated mean flow. Their competition allows for the first time to understand the experimentally observed bound dislocation pairs.

PACS numbers: PACS: 47.54.+r, 47.20.Ky, 47.20.Lz,

Striped patterns are ubiquitous in nature. They are found in physical, chemical, and biological systems, which are driven away from equilibrium [1]. In general natural patterns are not perfect due to the presence of defects, like grain boundaries (line defects) and topological point defects (dislocations) [2]. The nucleation, motion, and annihilation of dislocations is essential for many pattern-selection processes, which are initiated by modulational instabilities [1]. Dislocations govern the ordering kinetics of initially disordered patterns [3] and sustain in defect turbulent systems the perpetual reordering of the planforms [4]. Thus much effort has been devoted to the study of dislocations in striped patterns (see e.g. [1, 5, 6, 7]). Dislocations present a simple realization of topological singularities in a field description of continuous extended systems [8]. To which extent their dynamics can be understood in terms of "particles" subject to effective forces is a general important issue, that transcends pattern formation.

Here we study dislocations in Rayleigh-Bénard convection (RBC), which in the past has proven itself as a paradigm for pattern forming systems [1, 9]. In RBC a horizontal layer of a simple fluid is heated from below and cooled from above. For temperature differences  $\Delta T$  above a critical value  $\Delta T_c$ , buoyancy driven convection sets in typically in form of striped convection roll patterns with the critical wavenumber  $q = q_c$ . The basic hydrodynamic equations (Oberbeck-Boussinesq equations, OBE) are well established and the theoretical analysis can be quantitatively compared with well controlled experiments [9]. The communality of RBC with other bulk pattern-forming systems like, for example, vibrat-

ing granular layers [10], gas discharges [11], and Taylor-Couette flow [1] is most clearly expressed in universal model equations, like the Swift-Hohenberg (SH) equation [12] and its generalizations [13].

In this letter we concentrate on the dislocation dynamics in the case of gas convection, which over the past decade has attracted most interest [9]. Besides the appropriate SH-model, for the first time the full OBE equations are analyzed. We found the motion of dislocations to be driven by two independent "forces". One is the well known Peach-Koehler force, which describes the tendency of the system to develop towards a striped pattern with an optimal average wavenumber  $\bar{q} \approx q_c$  [5, 6]. Of particular importance is our explicit identification of a second non-potential force due to the advection of the dislocation core by its self-generated, roll-curvature driven mean flow. We demonstrate that this force acts in general to remove dislocations from the system as to reduce  $\bar{q}$ . The two forces may balance each other at a certain background wave number  $\bar{q} = q_D < q_c$ , such that the dislocation becomes stationary. For patterns with  $\bar{q} \gtrsim q_D$  the competition of the two forces can prevent the annihilation of two dislocations with opposite topological charge. This explains for the first time the experimentally observed bound dislocation pairs [14]. Although the significance of the mean flow had been expected for a long time in line with experiments [15], its direct identification in a previous theoretical analysis failed [16].

In RBC the strength of the mean flow is determined by the Rayleigh number  $R$  (a dimensionless measure of the temperature gradient across the convection cell) and in particular by the Prandtl number  $\sigma = \nu/\kappa$ , with the

kinematic viscosity  $\nu$  and the thermal diffusivity  $\kappa$ . Intermediate Prandtl numbers ( $\sigma \sim 1$ ) are realized in gas convection experiments [9]. In Fig. 1, a snapshot of the midplane temperature field  $\psi(x, y)$  containing a dislocation with positive topological charge  $Q = 2\pi$  from simulations of the OBE is shown.  $Q$  is defined via the winding number of the phase gradient  $\nabla\Phi(x, y)$  of  $\psi$  around a dislocation with the two possibilities  $\oint \nabla\Phi(x, y)ds = \pm 2\pi$ . The mean flow (arrows), which is driven by strong curvature of the rolls in the vicinity of the dislocation core, is maximal along the symmetry axis and tends to advect the dislocation downwards out of the system. In the direction perpendicular to the plane shown in Fig. 1 the mean flow shows an almost perfect parabolic profile.

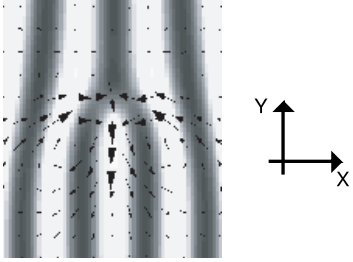


FIG. 1: Midplane temperature field (gray scale) of a dislocation with positive topological charge  $Q = 2\pi$  and the superimposed mean-flow velocity field (arrows). The dislocation is moving downwards along the  $y$ -axis. From simulations of the OBE for  $\epsilon \equiv (\Delta T - \Delta T_c)/\Delta T_c = 0.3$ ,  $\sigma = 1.2$  and background wavenumber  $\bar{q} = q_c$  (see text). A dislocation with  $Q = -2\pi$  would move upwards in this case.

While a comprehensive exploration of the  $R, \sigma$  parameter space within the OBE is extremely time consuming, we have gained much insight into the basic physical mechanism of dislocation dynamics by first studying the standard two-dimensional generalized SH-equations (GSH) [1, 6, 13]:

$$\partial_t \psi + (\vec{U} \cdot \nabla) \psi = [\epsilon_S - (1 + \nabla^2)^2] \psi - \psi^3, \quad (1)$$

$$\vec{U} = (U_x, U_y) = (\partial_y \xi, -\partial_x \xi), \quad (2)$$

$$(\partial_t - \nabla^2 + c) \nabla^2 \xi = g (\nabla (\nabla^2 \Psi) \times \nabla \psi) \cdot \vec{e}_z. \quad (3)$$

In terms of the two-dimensional field  $\psi(\vec{x}, t)$  the GSH-equations describe (in suitable dimensionless units) the bifurcation to patterns with critical wavenumber  $q_c = 1$  and their nonlinear saturation.  $\epsilon_S \propto \epsilon = (\Delta T/\Delta T_c - 1)$  measures the relative distance to onset. The coupling to the mean drift (or mean flow)  $\vec{U}(\vec{x})$  is characterized

by a coupling constant  $g$  (in RBC  $g \propto 1/\sigma$ ) and a cut-off parameter  $c$ . For  $g = 0$  the GSH-equations derive from a Lyapunov functional  $\mathcal{L}$  [1] and any dynamics is “downhill” towards the minimum of  $\mathcal{L}$ .

In our numerical analysis we focused on dislocation climb, *i.e.*, the motion parallel to the roll axis as shown in Fig. 1, in a rectangular domain  $-L_{x,y}/2 < x, y < L_{x,y}/2$  with width  $L_x$  and length  $L_y = 2L_x$ . We solved both the GSH- and the OBE equations numerically by a pseudo-spectral method with semi-implicit time stepping [17]. In order to minimize finite-size effects we have simulated dislocation pairs with periodic boundary conditions in the  $x, y$ - directions (Fig. 1 has to be extended mirror-symmetrically along the  $y$ -axis). We found, however, almost identical results for the less expensive simulations with a single dislocations in a box kept finite in the  $y$  direction by gradually ramping  $\epsilon$  to zero at  $y = \pm L_y/2$ . The ideal pattern without an immersed dislocation consisted of up to  $N = 64$  roll pairs of a wavelength  $\lambda = 2\pi/q_-$ , corresponding to  $L_x = N\lambda$ . The typical numerical resolution was  $\geq 8$  grid points per roll diameter. It is crucial to study systematically the defect dynamics as function of the background wavenumber  $\bar{q}$  of the underlying pattern. A superimposed dislocation leads to  $N + 1$  roll pairs in some parts of the cell (see Fig.1, below the dislocation) and consequently to a reduced wavelength  $\lambda_+ = N/(N + 1) \lambda$  and thus to a wavenumber  $q_+ = 2\pi/\lambda_+ > q_-$ . We found that defining the background wavenumber as  $\bar{q} = (q_+ + q_-)/2$  was most effective to absorb the finite- $N$  corrections. In designing the details of our calculational scheme and to validate our SH-code we have considerably profitted from the comparison with Ref. [6], devoted to the SH-model.

First we discuss the solutions of the GSH-equations. The simulations (for simplicity we consider the case of a single dislocation which climbs along the  $y$ -axis) were initialized with an approximate ansatz  $\psi(x, y, t = 0) \propto \cos[q_- x - \phi(|\vec{r}|)]$  at the center  $\vec{r}_0 = (x_0, y_0) = (0, 0)$  of the simulation domain. Here  $\phi(r)$  is the polar angle about  $\vec{r}_0$ . After the initial transients died out (say at  $|y - y_0| \gtrsim 4\lambda$  in Fig.1) the dislocation would climb with a constant velocity  $v_{st}$  and a relaxed asymptotic shape  $\psi(x, y, t) = \psi(x, y - v_{st}t)$  was reached. In subsequent runs, starting from this state considerably reduced the computational time. In agreement with prior investigations [6, 7], we have identified a wavenumber  $q_D(\epsilon, g)$ , such that for  $\bar{q} >$

$q_D$  the dislocation climbed downwards (the case shown in Fig. 1) with  $v_{st} < 0$  while it moved upward for  $\bar{q} < q_D$ .

The key for the physical interpretation of the results lies in a certain universality of  $\psi$  and  $\vec{U}$ . As demonstrated in Fig. 2A for a representative example of uniformly climbing dislocations at *fixed* background wave number  $\bar{q} = 0.98$  the numerical solutions  $\psi(x_0, \bar{y}) \equiv \psi_0(\bar{y})$  with  $\bar{y} = (y - v_{st}t)$  of Eq. 1 are virtually identical along the symmetry axis ( $x = x_0 = 0$ ) although the mean-field coupling  $g$  varies considerably ( $2 < g < 20$ ). In addition, as shown in Fig. 2B for the same range of parameters, the (suitably reduced) mean flow component  $U_y(x_0, \bar{y})/g$  along the symmetry axis has practically a  $g$ -independent shape  $U_0(\bar{y})$ , while the transverse component  $U_x$  vanishes for symmetry reasons. Inspection of Eq.(1) suggests that

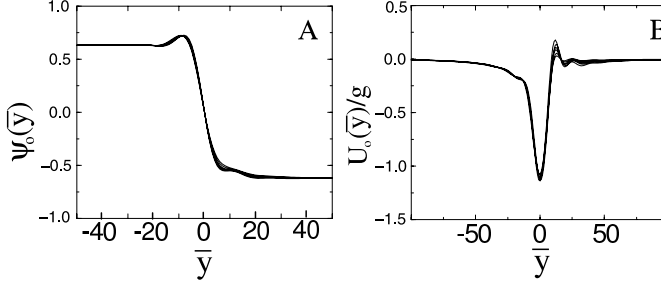


FIG. 2: Profiles of  $U_0(\bar{y}) \equiv U_y(x_0, \bar{y})/g$  and  $\psi_0(\bar{y}) \equiv \psi(x_0, \bar{y})$  plotted along the roll axis centered about the dislocation core at  $(x_0 = 0, \bar{y} = y - v_{st}t = 0)$  obtained from SH-simulations at  $\epsilon_s = 0.3$  and  $\bar{q} = 0.98$  in the range  $2 < g < 20$  for  $N = 16$ ,  $q_- = 0.95$  and  $c = 2$ . The profiles show approximately a fifth of the calculational grid of 512 pixels along  $\bar{y}$ , where 16 grid points correspond to length of  $3\lambda = 6\pi/q_-$ .

$\psi(x_0, \bar{y})$  can be well approximated by the potential solution  $\psi_0(\bar{y})$  at  $g = 0$ . This applies also to the source term in Eq. (3) with respect to its  $\psi$ -dependence. Thus Eq.1 on the symmetry axis reduces to:

$$-v_{st}\partial_{\bar{y}}\psi_0(\bar{y}) = -\frac{\delta\mathcal{L}}{\delta\psi_0(\bar{y})} + (U_y\partial_{\bar{y}})\psi_0(\bar{y}). \quad (4)$$

Averaging Eq.(4) over  $\bar{y}$  leads to the following relation for  $v_{st}$  as function of  $\bar{q}$  and  $g$ :

$$v_{st}(\bar{q}, g) = v_{pot}(\bar{q}, g \rightarrow 0) + c_1(\bar{q})gU_0^M \quad (5)$$

With respect to the advection term, we have made explicit the (reduced) mean flow  $U_0^M$  at the dislocation core (i.e. the minimum of  $U_0(\bar{y} = 0)$  in Fig. 2B), which dominates the average in Eq. (4) also because of the strong maximum of  $\partial_{\bar{y}}\psi_0(\bar{y})$  at  $\bar{y} = 0$  (see Fig. 2 A) [18]. The

quantities  $v_{pot}, c_1$  and  $U_0^M$  have to be determined numerically as function of  $\bar{q}$  and  $\epsilon_s$ .

For clarity the consequences of Eq. (5) are discussed for  $Q = 2\pi$  (see Fig. 1), since the case  $Q = -2\pi$  is analogous. The potential or Peach-Koehler contribution  $v_{pot}$ , originating from the functional derivative of  $\mathcal{L}$  in Eq. (4), is negative for  $\bar{q} > q_c = 1$ , vanishes for  $\bar{q} \approx q_c$ , and becomes positive for  $\bar{q} < q_c$ . Thus the dislocation climbs as to move the wavenumber of the pattern in its wake towards an optimal value  $q_{opt} \approx q_c$ , where the potential energy has its minimum [5]. Since  $c_1(\bar{q})$  in Eq.(5) was found to be always positive for all  $\bar{q}$  and  $\epsilon_s$ , the mean flow ( $\propto U_0^M < 0$ ) would always advect the dislocation such as to decrease the wavenumber  $\bar{q}$ . In fact, for  $g \neq 0$  in patterns with  $\bar{q}$  in the range  $q_D \leq \bar{q} \leq q_{opt}$  the potential contribution  $v_{pot}$  is overcome by the mean flow contribution leading to  $v_{st} < 0$ . At  $\bar{q} = q_D(\epsilon, g)$  both effects cancel leading to a immobile dislocation ( $v_{st} = 0$ ). In agreement with prior investigations [6] our numerical results show that  $v_{st}$  varies almost linearly as function  $\bar{q}$  according to  $v_{st} \propto (\bar{q} - q_D)$  over a wide  $\bar{q}$ -range for fixed  $g > 0$  and  $\epsilon_s > 0$ . According to Eq.(5) this implies at fixed  $\bar{q}$  a linear dependence of  $v_{st}$  on  $g$ , which was numerically confirmed in a wide  $g$ -range ( $0 \leq g \leq 30$ ).

Although in full hydrodynamics (OBE) a direct analog of potential  $\mathcal{L}$  in the GSH is not defined, the reasoning in terms of a potential force ( $\sigma \rightarrow \infty$ ) and a competing mean flow force seems to apply well. As a typical example for  $\sigma = 1.4$ , we show in Fig. 3A the linear variation of  $v_{st}(\bar{q})$  as function of  $\bar{q}$ , which crosses  $v_{st} = 0$  at  $\bar{q} = q_D = 2.75$ . In Fig. 3B it is demonstrated, that  $v_{st}$  varies like the SH-results linearly in  $\sigma^{-1} \sim g$  at fixed  $\bar{q}$ . Our findings are in perfect agreement with the experimental and numerical analysis of the dynamics of the off center "giant spirals" [7] for  $\sigma \approx 1$  where the uniformly rotating outer tip would probe roll patches in a fairly large  $\bar{q}$ -range.

In agreement with experiment [14], from equation (5) the possibility of bound dislocations pairs is obvious. A well separated pair of oppositely charged dislocations on a background pattern with  $q_D < \bar{q} < q_c$ , is driven by the dominant mean-flow contribution  $\propto |U_0^M|$  in Eq. (5) towards their annihilation. However, this advection force weakens continuously, as the opposing mean flow contributions from each dislocation begin to overlap destructively. Eventually the dislocations stop moving, when the

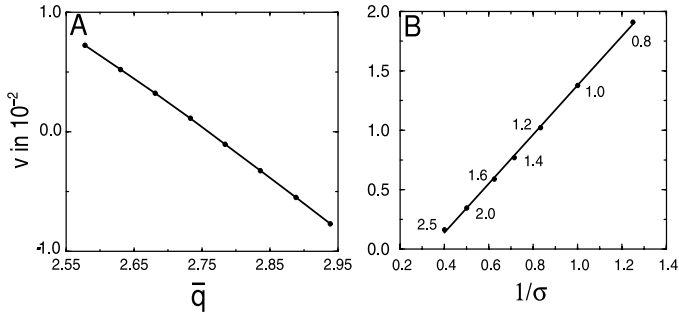


FIG. 3: Dislocation velocity  $v_{st}$  in units of  $10^{-2}d/t_v$  with  $d$  the cell width, and  $t_v = d^2/\kappa$  the vertical diffusion time. A: as function of  $\bar{q}$  at fixed  $\sigma = 1.4$ . B: as function of  $\sigma$  in the range  $0.8 \leq \sigma \leq 2.5$  of at  $\bar{q} = 2.91$ , data from simulations of the OBE for  $\Delta T/\Delta T_c - 1 = 0.3$ .

reduced advection force is balanced by the opposing potential force. To our surprise even the deceleration of the approaching dislocations was well captured adiabatically by Eq. (5), derived under the assumption of constant  $v_{st}$ . In fact, we found a direct proportionality between the decreasing velocity  $v(t)$  of the approaching dislocations and the resulting  $U_0^M(t)$ . The equilibrium distance  $l_D$  of the dislocations in the bound pair as function of  $\bar{q}$  and  $g$ , or  $\sigma$ , respectively, has not been investigated systematically. However, typically we find  $l_D \sim 2 - 3\lambda$  [19].

In our OBE and GSH-simulations dislocations are found to be very robust objects except when  $\bar{q}$  lies in the vicinity of a cross-roll (CR) instability boundary [21] for ideal rolls, e.g. in the OBE near  $\bar{q} = 2.48 < q_c = 3.11$  for  $\sigma = 1.4, \epsilon = 0.3$ . Then, as in the experiments [9, 20] the dislocation core might split into a chain of bubbles by a localized transverse bridging of adjacent rolls. This local CR instability has been described at first in the SH-model simulations [22], but we doubt that the dislocation mechanism invoked there has a merit.

In conclusion, we have presented an analysis of the defect dynamics for medium  $\sigma$  and finite  $R$  in RBC, which has allowed to separate clearly potential- and mean-flow forces. Our main interest was to elucidate the basic mechanism. Details, like for instance the dependence of  $q_D$  on  $\sigma$  and  $\epsilon$  and the impact of the stability properties of the background pattern will given in a separate manuscript. We expect that our methodology, to separate potential and nonpotential effects will be applicable as well to a number of other systems that show striped patterns as mentioned before. E.B. is grateful for support from the National Science Foundation under grant

DMR0072077.

- 
- [1] For a comprehensive review on pattern forming instabilities, see for example: M. C. Cross and P. C. Hohenberg, *Rev. Mod. Phys.* **65**, 851 (1993) and references therein.
  - [2] A. C. Newell, T. Passot and J. Lega, *Annu. Rev. Fluid. Mech.* **25**, 399 (1993).
  - [3] See e.g.: C. Harrison et al., *Science* **290** 1558 (2000); L. Purvis and M. Dennin, *Phys. Rev. Lett.* **86**, 5898 (2001);
  - [4] K. Daniels and E. Bodenschatz, *Phys. Rev. Lett.* **88** 034501 (2002) and references therein.
  - [5] E. D. Siggia und A. Zippelius, *Phys. Rev. A* **24** 1036, (1981).
  - [6] G. Tesauro und M. C. Cross, *Phys. Rev. A* **34**, 1363 (1986).
  - [7] B. Plapp, D. Egolf, E. Bodenschatz, and W. Pesch, *Phys. Rev. Lett.* **81**, 5334 (1998).
  - [8] L. M. Pismen, “Vortices in nonlinear fields” Clarendon Press, Oxford, 1999.
  - [9] See e.g, E. Bodenschatz, W. Pesch, and G. Ahlers, *Annu. Rev. Fluid Mech.* **32** 709 (2000) and references therein.
  - [10] J.R. de Bruyn et al. , *Phys. Rev. Lett.* **81** 1421 (1998).
  - [11] Y.A. Astrov et al., *Phys. Rev. Lett.* **80** 5341 (1998).
  - [12] J. Swift und P. C. Hohenberg, *Phys. Rev. A*, **15**, 319 (1977) .
  - [13] P. Manneville, *J. Physique* **44**, 759 (1983); H. S. Greenside and W. M. Coughran, *Phys. Rev. A* **30**, 398 (1984).
  - [14] See e.g. : E. Bodenschatz et al. *Physica D* **61** 77 (1992); B. Plapp, PhD thesis, Cornell 1997.
  - [15] A. Whitehead, *J. Fluid. Mech.* **75**, 715 (1976).
  - [16] See the discussion in [5], where the OBE were solved, however, in a fairly small system with unrealistic free-slip boundary condition.
  - [17] W. Pesch, *Chaos* **6**, 348 (1996).
  - [18] For numerical reasons it is easier to characterize the mean-flow strength at the dislocation core by the average of the profile  $U_0(y)$  along  $y$ , which is obviously proportional to  $U_0^M$ .
  - [19] In the OBE simulations we found bound states for  $\epsilon = 0.3, \sigma = 1.4$  in a regime  $2.79 < q < 2.64$  slightly above  $q_D = 2.75$  (calculation with 16 rolls on a  $256 \times 512$  grid).
  - [20] M. Assenheimer and V. Steinberg, *Nature* **367**, 345 (1994).
  - [21] F. H. Busse, *Rep. Prog. Phys.* **41**, 1929 (1978).
  - [22] A. C. Newell and T. Passot, *Phys. Rev. Lett.* **68** 1846 (1992). The simulations were performed just at the CR instability line ( $q_{cr} = 1.5 > q_c$  for  $\epsilon_S = 3$ ). In our larger integration domain with controlled initial conditions, we found no indication of their resonant  $q/3$  process.